IV. AXIAL DISPERSION MODEL

A. Introduction

The analysis which begins below is a follow-up report to the tanks-in-series analysis. R. E. Larson examined the same tracer data in terms of an axial dispersion model [15]. Although the tanks-in-series analysis was useful, a dispersion model offers the additional benefit of scaleability. The principal results of this study are the values of the axial dispersion coefficient in both the liquid and gas phases. The effects of phase transfer are taken into account in the measurement of gas phase dispersion, and a measure of the Henry's law constant for argon in the slurry is given. An effective dispersion coefficient is calculated from the liquid and gas coefficients and translated to the number of effective CSTR's in series. This analysis and data provides a method to determine the degree of dispersion in the LPMEOH reactor for use in scale-up.

B. Background: Axial Dispersion Model

The mixing characteristics of the LaPorte slurry bubble column reactor are not expected to be simple. The reactor is currently operated batch-wise with respect to the slurry, neglecting a small loss of mineral oil overhead and consequent retrieval and makeup (about 0.226 gal/min, or 2×10^{-4} ft/sec superficial velocity). Gas enters the reactor through a sparger at the bottom of the reactor. At some height above the sparger, a bubble size and radial distribution of gas may be achieved which are not greatly influenced by the sparger.

In the upper section of the column, a flow pattern which is driven by the buoyancy of the gas phase is probably established. The largest scale of this flow, often referred to as gulf streaming, has been observed in bubble columns to consist of a number of circulation cells limited in size by the radius of the column [8].

Despite the complexities of the actual mixing process, the full simplicity of the dispersion model is retained and the mixing of the liquid phase is described in terms of uniform dispersion along the entire slurry height. The mixing of the gas phase is also described as uniform dispersion superimposed upon plug flow. This simplicity makes scale-up of the model possible. Like the tanks-in-series model, the dispersion model is phenomenological. It is very useful as a description of the mixing, adequate for reactor design, but it is not a faithful representation of the complexities of the actual flow.

One advantage of the dispersion model over the tanks-in-series model is that detector responses at several axial positions along the reactor can be matched for each injection. Tracer signals were, in fact, measured at several heights along the reactor vessel as a basis for measuring both liquid and gas phase mixing. The tanks-in-series model utilized only the data from the inlet, outlet and slurry level detectors.

Radioactive argon, which was used as the gas phase tracer, dissolves significantly into the liquid. Phase transfer must therefore be accounted for in an attempt to characterize the gas phase mixing from argon tracer data. The inherent gas phase dispersion coefficient can be estimated, however, from the overall effective dispersion of argon by making use of the independently measured liquid phase dispersion coefficient.

1. Axial Dispersion Liquid Mixing Model

For the liquid slurry, considered a batch system, the concentration of tracer at any axial position is modeled by

$$\mathcal{D}_L \frac{\partial^2 C}{\partial Z^2} = \frac{\partial C}{\partial t} \quad , \quad t > to \; , \; 0 \leq Z \leq L \qquad (16)$$

where C(z,t) is the radially averaged concentration of tracer at axial position z, time t. The axial dispersion coefficient, $\mathcal{D}_L$, has units of diffusivity, length^2/time.

The initial condition for a pulse injection is $C(z,t_o) = \delta(z)$, and the boundary conditions for $t > t_o$ are $\partial C/\partial z = 0$ at $z = 0$ and $z = L$. $\delta(z)$ is the Dirac delta function centered on $z = 0$. The solution is:

$$\frac{C}{Co} = 1 + \sum_{n=1}^{\infty} 2 \cos\left(\frac{N\pi Z}{L}\right) \exp\left[-\frac{N^2\pi^2(t-to)\mathcal{D}_L}{L^2}\right] \qquad (17)$$

C_o is the final concentration of tracer, uniform throughout the column. (See Appendix D for the derivation.) The normalized response curves from the radiation detectors are equated to C/C_o, a good assumption under sufficient radial mixing.

The injection pulse was also measured with a detector mounted on the injection line as close to the reactor vessel as possible. The finite width and shape of this pulse are taken into account by summing the ideal response over a series of impulse functions of appropriate weight.

A computer program was written which carries out the model calculations for a given injection pulse and dispersion coefficient. A visual fit of the two injections is sufficient to

find the best possible fit of the data. A least squares fit of the dispersion coefficient would be appropriate if more data were available or more accuracy possible. However, with 8 of the detectors failing on the first injection and the second injection being, in reality, the injection of the residual powder from the first attempt which remained in the inlet line, the accuracy of the detector data would not merit these numerical fits.

2. Axial Dispersion Gas Phase Mixing Model

The model equation for dispersion under plug flow, applied to the gas phase, is

$$\mathscr{D}_G \frac{\partial^2 C_G}{\partial Z^2} - \frac{U_G}{\epsilon_G} \frac{\partial C_G}{\partial Z} + K_L a \, (HC_L - C_G) = \frac{\partial C_G}{\partial t} \qquad (18)$$

U_G is the superficial gas velocity and ϵ_G is the gas phase volume fraction. An interphase transfer term is included: (K_L a) is the mass transfer coefficient and H is the Henry's Law coefficient. Dispersion in the gas phase is coupled with dispersion in the liquid by the following:

$$\mathscr{D}_L \frac{\partial^2 C_L}{\partial Z^2} - \frac{\epsilon_G}{\epsilon_L} K_L a \, (HC_L - C_G) = \frac{\partial C_L}{\partial t} \qquad (19)$$

Phase transfer does not affect the superficial concentration $\epsilon_G C_G + \epsilon_L C_L$, so multiplying (18) by ϵ_G and (19) by ϵ_L and adding eliminates the term. Assuming mass transfer resistance is small, $C_G = H C_L$ at every point. This simplifies to (See Appendix E):

$$\mathscr{D}_{EFF} \frac{\partial^2 C_G}{\partial Z^2} - U_{EFF} \frac{\partial C_G}{\partial Z} = \frac{\partial C_G}{\partial t} \qquad (20)$$

where

$$\mathscr{D}_{EFF} = \frac{\mathscr{D}_G + \frac{\epsilon_L}{H\epsilon_G} \mathscr{D}_L}{1 + \frac{\epsilon_L}{H\epsilon_G}} \qquad (21)$$

and

$$U_{EFF} = \frac{U_G}{\epsilon_G + \frac{\epsilon_L}{H}} \qquad (22)$$

Equation (20) is simply the plug flow dispersion equation. Here ϵ_L is the overall volume fraction of liquid in the dispersion, equal to $[(1-\epsilon_G)(1-\epsilon_{SL})]$ where ϵ_{SL} is the fractional volume of solids in the slurry. The first term, $(1-\epsilon_G)$ represents the fraction of the slurry volume divided by the total volume and the second term, $(1-\epsilon_{SL})$, is the volume fraction of liquid in the slurry.

The solution of (3), due to Brenner [4,6], is (See Appendix F)

$$C = \bar{C} \sum_{n=1}^{\infty} f_n \exp\left(-A_n(t-t_o)\mathscr{D}_{EFF}/L^2\right) \qquad (23)$$

$$f_n = \frac{8\,\alpha_n}{4\,(\alpha_n^2 + Pe) + Pe^2}\left(\alpha_n \cos\frac{\alpha_n Z}{L} + \frac{Pe}{2}\sin\frac{\alpha_n Z}{L}\right)\exp\left(\frac{PeZ}{2L}\right) \qquad (24)$$

$$A_n = \alpha_n^2 + \frac{Pe^2}{4} \qquad (25)$$

$$Pe = \frac{U_{EFF}\,L}{\mathscr{D}_{EFF}} \qquad (26)$$

where α_n are the positive roots, taken in order, of

$$\frac{\alpha_n}{2}\tan\left(\frac{\alpha_n}{2}\right) - \frac{Pe}{4} = 0 \qquad (27)$$

and

$$\frac{\alpha_n}{2}\cot\left(\frac{\alpha_n}{2}\right) + \frac{Pe}{4} = 0 \qquad (28)$$

respectively.

This solution is for a pulse input at time t_o, and $z = 0$. The boundaries are closed: the boundary conditions are $C_G U_{EFF} = \mathscr{D}_{EFF}\,\partial C/\partial z$ at $z = 0$ and $\partial C/\partial z = 0$ at $z = L$. The latter boundary condition is an approximation which ensures that the solute concentration does not pass through a minimum or a maximum while in the slurry.

The normalization factor $\bar{C}$ is the integral of concentration at a fixed height with respect to dimensionless time:

$$\bar{C} = \frac{U_{EFF}}{L} \int_{to}^{\infty} C(L,t)\, dt \qquad (29)$$

Where to is the time of injection

The model requires that two adjustable parameters, $\mathcal{D}_{EFF}$ and U_{EFF}, be simultaneously fit to the actual response curves.

Consistent with the tanks-in-series analysis, the freeboard region of the reactor is treated as a plug flow reactor. Model response curves for those detectors above the slurry height, ie., $z > L$, are taken as equivalent to that at $z = L$ shifted in time by $t_{LAG} = (z-L)/U_G$. A very small time shift is included for the time it takes the tracer to pass from the injection detector to the sparger.

As with the liquid tracer, the injection pulse was monitored with a detector mounted on the injection line. The finite time span of injection is again taken into account by summing the ideal pulse response over a series of impulse functions of appropriate weight.

A computer program was developed which carries out the simultaneous fit of dispersion coefficient and bulk velocity. The sum of the squares of residuals between the model and an actual detector response curve are calculated as a function of dispersion coefficient and bulk holdup time.

Several of the detectors appear to have been faulty or to simply not fit the model very well. As a basis for disregarding certain detectors, it is assumed that only fits for which the sum of squares is within a certain tolerance represent a valid fit.

Note that by rearranging equation 22, the Henry's Law coefficient for argon may be calculated from the tracer data by the effective velocity, along with the measurements of gas holdup:

$$H = \frac{\varepsilon_L\, U_{EFF}}{U_G - \varepsilon_G\, U_{EFF}} \qquad (30)$$

H varies between zero and infinity as U_{EFF} varies between zero and U_G/ε_G.

C. Axial Dispersion Model Fit

1. Liquid Phase Measurements

Dispersion coefficients were fit first to the liquid tracer data. These data were taken at the conditions listed in Table IV.C.1-1

as case 7. Response curves were first smoothed by Laplace transform filtering [1], then added together at a given height. Figures IV.C.1-1, IV.C.1-2, IV.C.1-3, and IV.C.1-4 show the response curves out to 120 seconds. Five positions are given: z = 44, 86, 140, 188, and 230 inches above the reactor bottom. Note that, except for the detector at 44 inches, the fit is reasonably good and seems to fall between the two values of dispersion coefficient plotted, $\mathscr{D}_L = L^2\ 0.008\ sec^{-1}$ and $\mathscr{D}_L = L^2\ 0.009\ sec^{-1}$, or $\mathscr{D}_L = 3.7 \pm 0.2\ ft^2/sec$. This fit is best for the uppermost detectors.

Several correlations exist in the literature for liquid dispersion coefficients measured primarily in bubble columns. The three-phase slurry bubble column is an extension of the two-phase column discussed in the literature, particularly in the limit of very small solid particle sizes. However, most of the data reported in the literature is for small diameter reactor systems operating at superficial gas velocities below those of the LaPorte reactor.

Akita [7] measured dispersion in 3.0, 6.0, and 11.9 inch diameter bubble columns of air in various liquids and presented a correlation for the experimental data:

$$\frac{\mathscr{D}_L}{DU_G} = \frac{(Dg)^{1/2}}{U_G}\left[0.06 + 0.55\left(\frac{U_G}{(Dg)^{1/2}}\right)^{0.7}\right] \qquad (31)$$

Baird and Rice [3,12] showed the following correlation by dimensional analysis:

$$\frac{\mathscr{D}_L}{DU_G} = K\left[\frac{(Dg)^{1/2}}{U_G}\right]^{2/3} \qquad (32)$$

and set K = 0.35 according to a fit of literature data. The tabulated data included bubble columns as large as 17.3 inches in diameter operated at superficial gas velocities as high as .67 ft/sec.

The two correlations above both predict $\mathscr{D}_L$ near 2.0 ft^2/sec, 45% low relative to the measurement for case 7. The scatter in the data to which the correlations are fit is about 50%, and it is interesting that both correlations also underpredict the dispersion for the larger columns tabulated by Baird and Rice.

TABLE IV.C.1-1
REACTOR CONDITIONS FOR EACH INJECTION

	Injection #	Inlet Superficial Gas Velocity ft/sec	Outlet Superficial Gas Velocity ft/sec	Slurry Level [*] ft	Gas Holdup	Catalyst Inventory (Oxide) kg	Solids Holdup Overall (Reduced Catalyst)	Solids Holdup in Slurry
Case 1	1	0.25	.209	18.08	0.286	362	0.036	0.050
	2			18.08	0.286	362	0.036	0.050
	3			18.00	0.286	362	0.036	0.050
Case 2	4	0.50	.415	19.83	0.363	362	0.033	0.051
	5			19.75	0.363	362	0.033	0.051
	6			19.75	0.363	362	0.033	0.051
Case 3	7	0.60	.504	20.16	0.378	362	0.032	0.052
	8			19.91	0.378	362	0.032	0.052
	9			19.91	0.378	362	0.032	0.052
	10			19.75	0.378	362	0.033	0.053
Case 4	1B	0.50	.435	13.91	0.353	256	0.033	0.051
	2B			13.91	0.353	256	0.033	0.051
	3B			13.83	0.353	256	0.033	0.051
Case 5	4B	0.25	.224	12.41	0.273	256	0.037	0.051
	5B			12.25	0.273	256	0.037	0.051
	6B			12.25	0.273	256	0.037	0.051
Case 6	7B	0.19	.171	11.66	0.227	256	0.039	0.051
	8B			11.66	0.227	256	0.039	0.051
	9B			11.66	0.227	256	0.039	0.051
Case 7	1L	0.50	.415	20.67	0.439	301	0.026	0.036
	2L			20.75	0.439	301	0.026	0.036

Reactor Temperature: 482° ±5°F
Reactor Pressure: 753 psig

* relative to reactor bottom

FIGURE IV.C.1-1

Signal - First Pulse

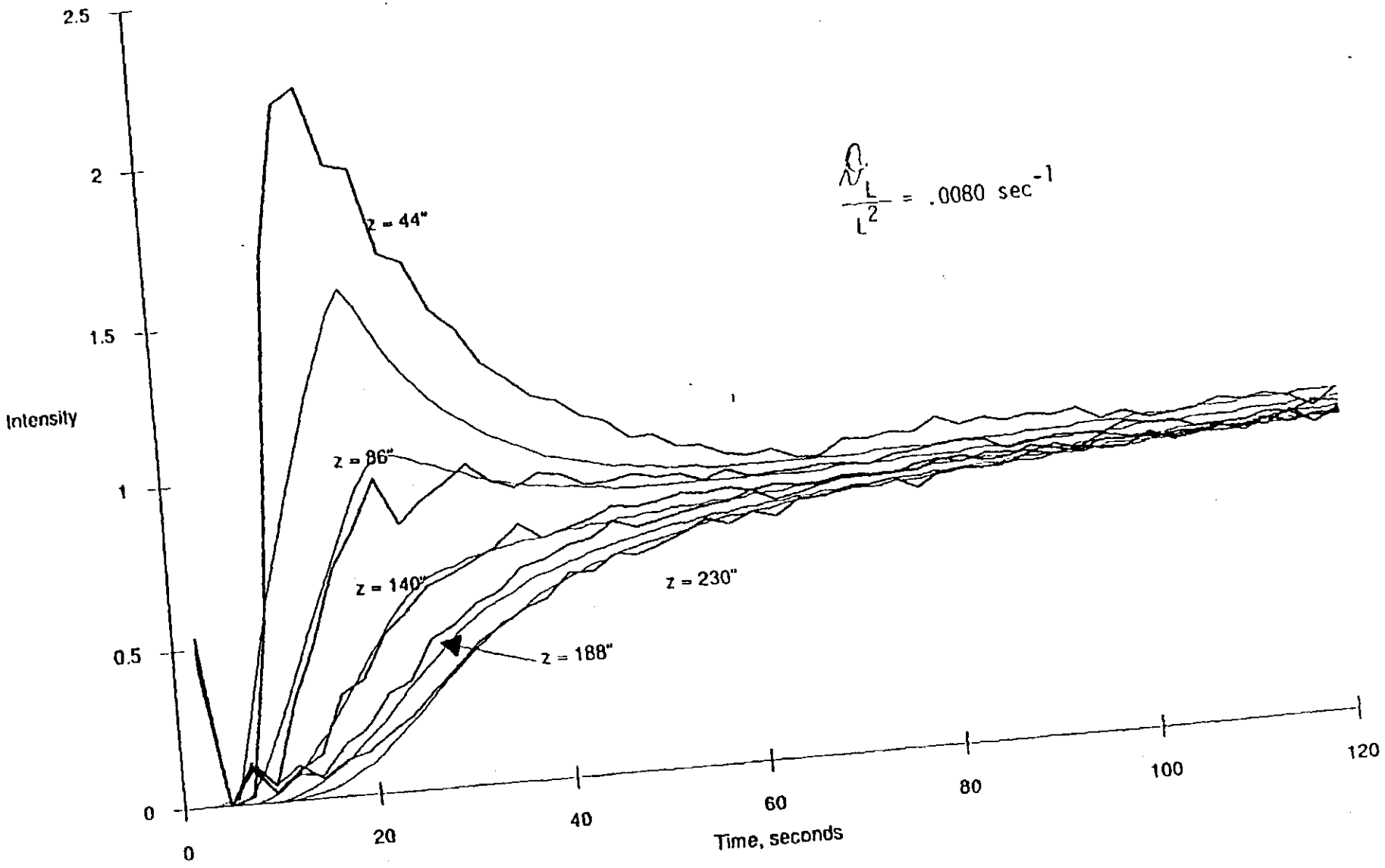

FIGURE IV.C.1-2

Signal - First Pulse

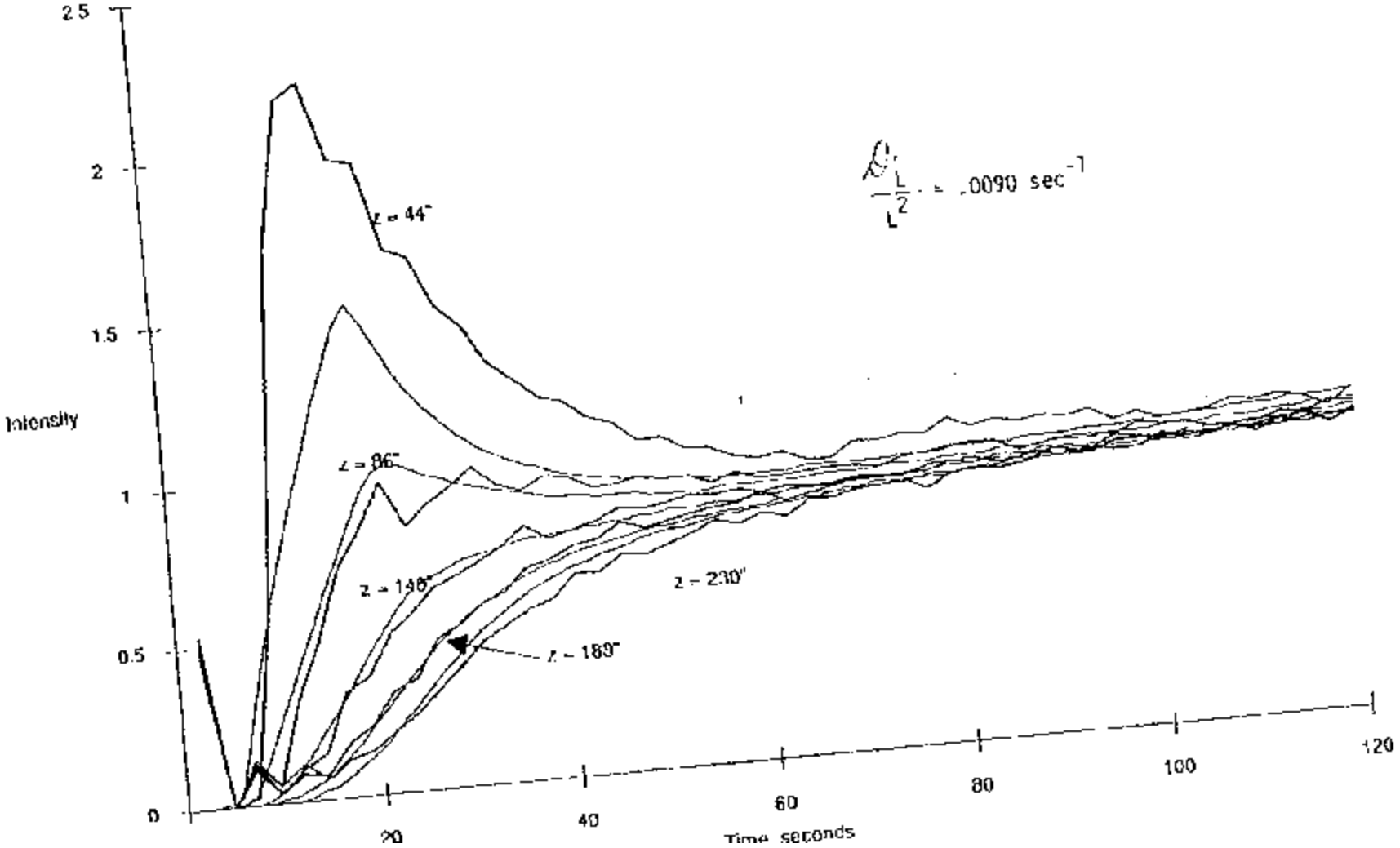

$$\frac{D}{L^2} = .0090 \text{ sec}^{-1}$$

FIGURE IV.C.1-3

Signal - Second Pulse

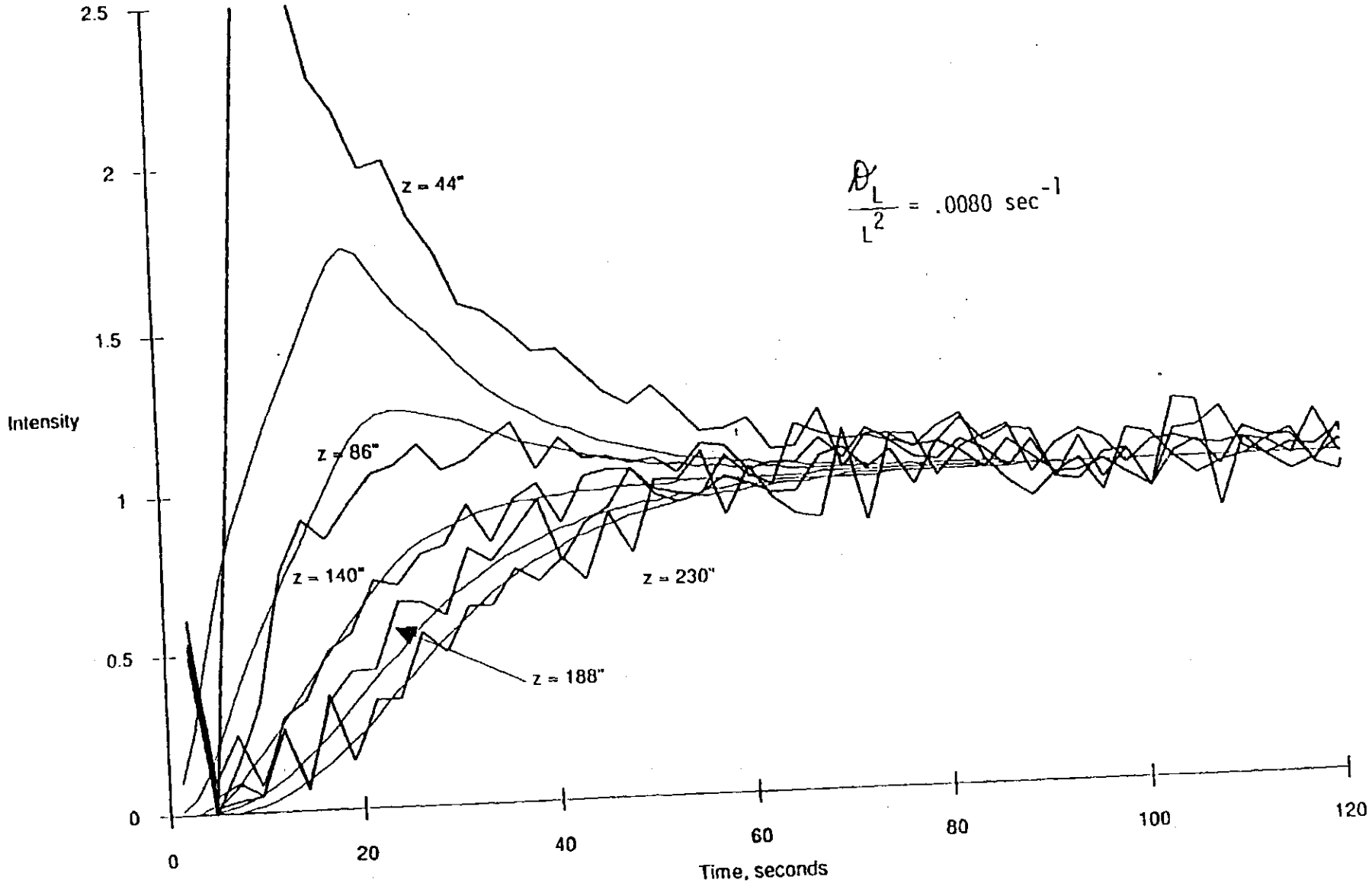

FIGURE IV.C.1-9

Signal - Second Pulse

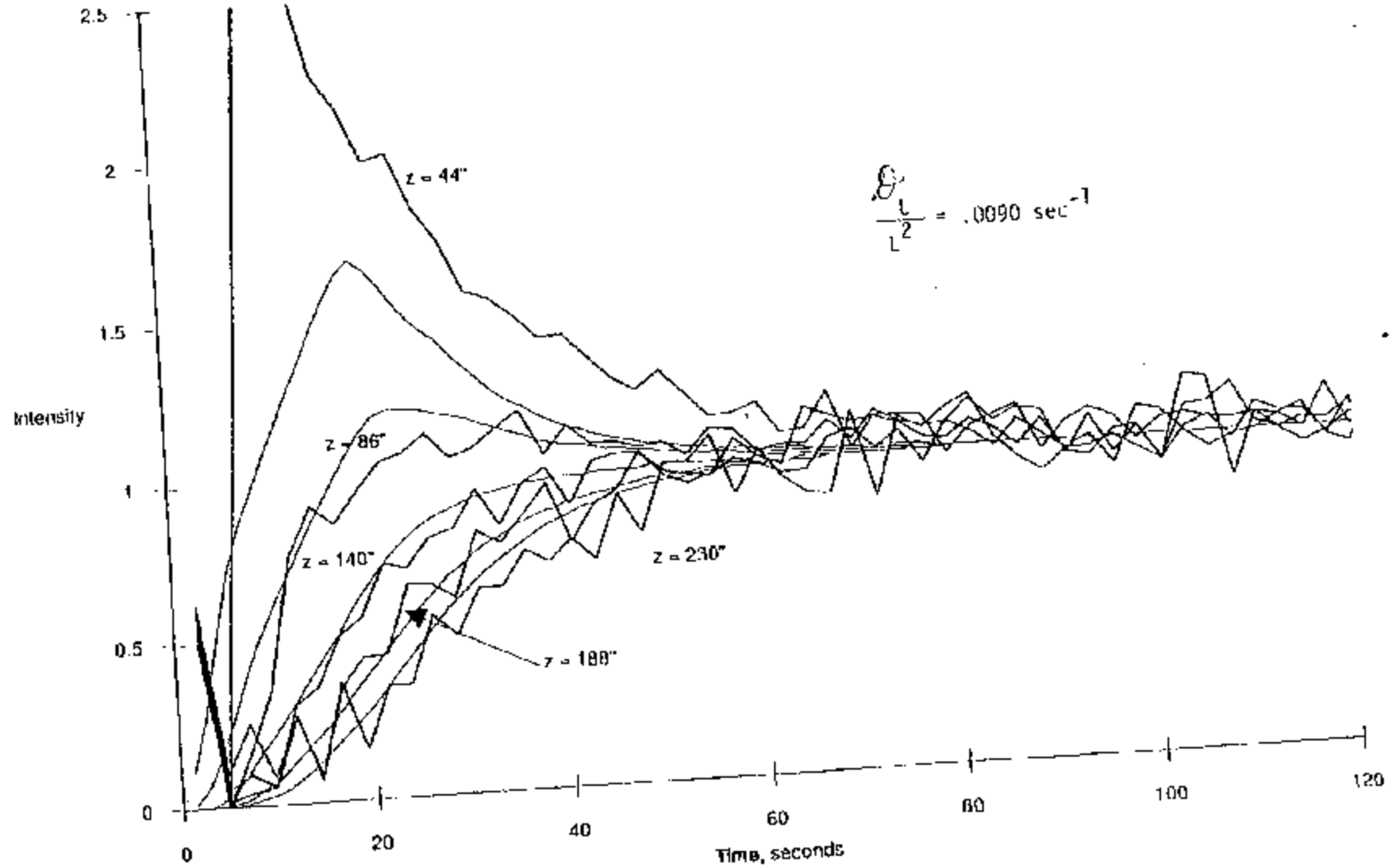

Matsumoto et al. [9,10] derived a mechanistic equation for $\mathscr{D}_L$ based on mixing length theory. This equation, in the limit of zero bulk liquid velocity, is

$$\mathscr{D}_L = K\,(gD^3\,\varepsilon_G)^{1/2} \qquad (33)$$

K = 0.3 is given, again fit to two-phase bubble column data. For the diameter of the LaPorte column and a gas holdup value as measured for case 7, this correlation gives a value of 2.89 ft^2/sec, 38% low relative to the measurement.

The first two correlations, (31) and (32), are in close agreement in the neighborhood of our test conditions and suggest an extrapolation of the dispersion coefficient proportional to $D^{4/3}U_G^{1/3}$. The third correlation, (33), suggests an extrapolation of $\varepsilon_G^{1/2}D^{3/2}$ which is not a simple function of superficial gas velocity since the gas holdup, ε_G, is also a function of slurry properties. Since the data from LaPorte did not test a wide range of gas holdups, a correlation of the form suggested by Baird and Rice (equation 32) is recommended.

2. Gas Phase Measurements

The quantity of data available from gas tracer measurements made a more rigorous fit of the data possible. The dispersion coefficients and slurry holdup times for each detector are given in **Appendix G**. The norm of residuals may vary between 0 (a perfect fit) and 1. Certain fits must be rejected so that a dispersion coefficient is chosen based only on those response curves that fit the model quite well. As indicated in the last column of **Appendix F**, any detector for which the norm of residuals is greater than 0.09 is rejected. The remaining fits are averaged and tabulated in **Table IV.C.2-1**.

Figure IV.C.2-1 is a plot of the averaged dispersion coefficient for each injection. $\mathscr{D}_{EFF}$ varies between about 1.5 ft^2/sec and 3 ft^2/sec, increasing with increasing superficial gas velocity. The value of $\mathscr{D}_L$, for dispersion due to liquid mixing alone, measured for case 7 is also shown in **Figure IV.C.2-1**. From this point, an extrapolation was made according to the dependence suggested by Baird and Rice, ie., $\mathscr{D}_L$ proportional to $U_G^{1/3}$. This approximation of the liquid dispersion as a function of superficial gas velocity is shown as a dashed line. The plot shows that the mixing due to the liquid phase is more intense than that measured by the gas tracer.

TABLE IV.C.2-1
Averaged Results for Effective Dispersion

	Injection	D/(L*L) Average (1/sec)	M.R.T. Average (sec)	D/(L*L) Std Dev (1/sec)	M.R.T. Std Dev (sec)	Number of Detectors Used
Case 1	1	0.00646	47.8	0.00102	7.5	11
	2	0.00621	44.7	0.00109	9.0	10
Case 2	3	0.00590	41.7	0.00057	5.8	4
	4	0.00733	25.3	0.00124	3.4	9
	5	0.00813	25.4	0.00154	3.7	9
	6					0
Case 3	7	0.00863	22.3	0.00150	2.7	6
	8	0.00846	22.3	0.00201	2.9	6
	9	0.00812	21.1	0.00133	1.4	6
	10	0.00809	21.6	0.00162	1.1	3
Case 4	1b	0.01337	16.5	0.00161	1.9	6
	2b	0.01412	17.2	0.00053	1.3	4
	3b	0.01464	16.3	0.00277	1.5	7
Case 5	4b	0.00954	23.7	0.00131	2.6	4
	5b	0.01186	23.3	0.00110	1.9	4
	6b	0.01095	23.5	0.00177	2.9	2
Case 6	7b	0.01150	38.9	0.00224	16.5	5
	8b	0.01307	35.2	0.00522	11.1	5
	9b	0.01001	30.2	0.00125	3.8	4

FIGURE IV.C.2-1

Effective Dispersion vs Outlet Superfical Gas Velocity

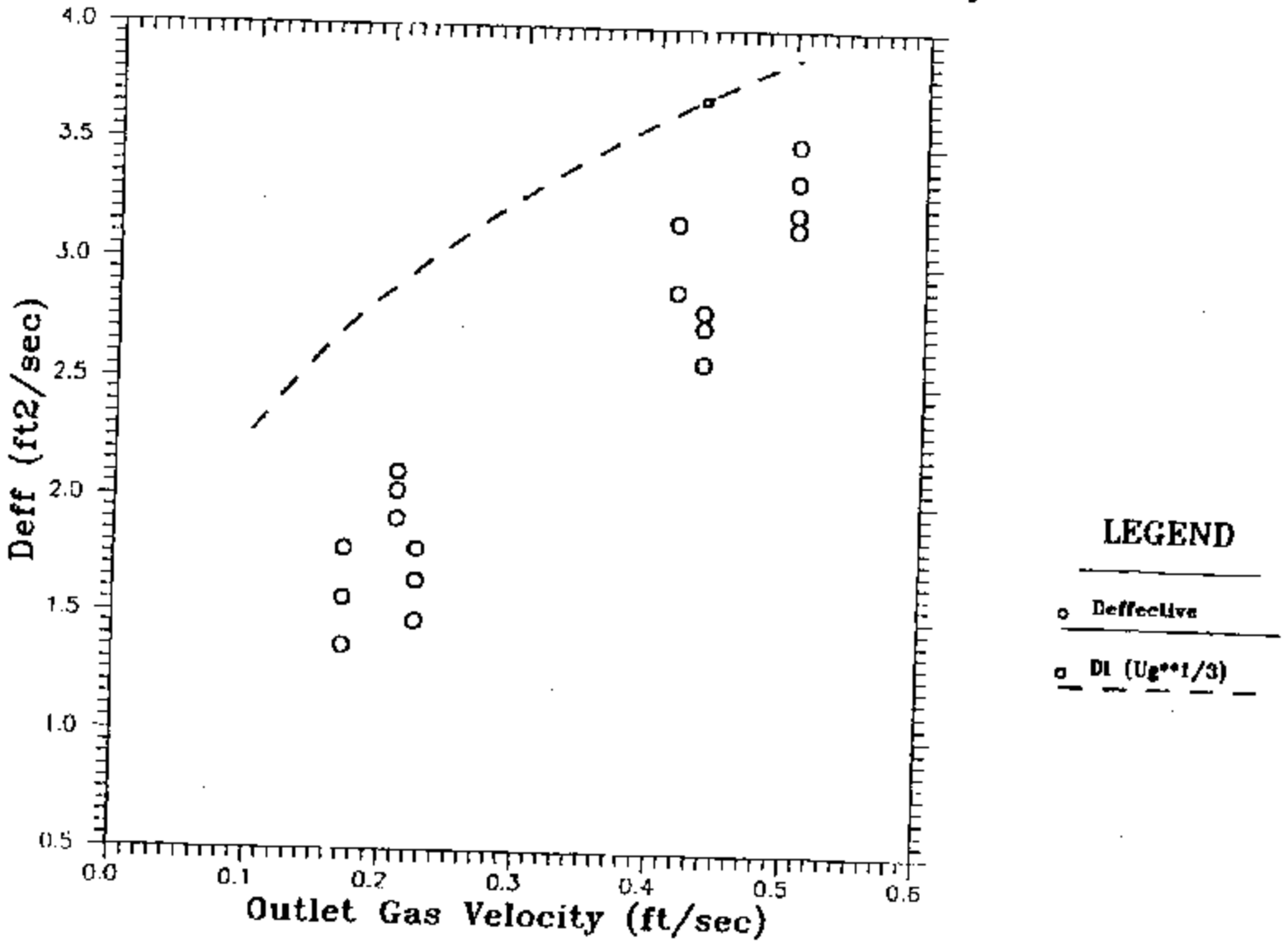

We calculate the gas dispersion coefficient, $\mathscr{D}_G$, using the definition of $\mathscr{D}_{EFF}$:

$$\mathscr{D}_G = \mathscr{D}_{EFF}(1+\eta) - \eta\mathscr{D}_L \quad , \quad \eta = \frac{U_G - \varepsilon_G U_{EFF}}{\varepsilon_G U_{EFF}} \qquad (34)$$

Values of $\mathscr{D}_G$ are plotted in **Figure IV.C.2-2** for the individual injections as a function of superficial gas velocity. One injection gives a slightly negative dispersion coefficient, an anomoly due to the combination of experimental error and uncertainty in the prediction of the liquid phase dispersion. On average, $\mathscr{D}_G$ roughly follows a $U_G^{3/2}$ curve, and varies between zero and 3.5 ft^2/sec.

There are few correlations in the literature for dispersion coefficients in the gas phase. For a recent review of the available correlations, see Fan [11] p.270. These correlations are made largely from air-water data, and they predict gas phase mixing far greater than that measured in our system. As an example, Field and Davidson [2] give

$$\mathscr{D}_G = 1.82\, D^{1.33\left(\frac{U_G}{\varepsilon_G}\right)^{3.56}} \qquad (35)$$

(D - units of feet)
(U_G - units of feet/second)

For our system, at U_G = 0.5 ft/sec and ε_G = 0.363 (case 2), this predicts a $\mathscr{D}_G$ = 12.33 ft^2/sec. Towell and Ackerman [12] give

$$\mathscr{D}_G = 6.0\, D^2\, U_G \qquad (36)$$

(D - units of feet)
(U_G - units of feet/second)

For our system, at case 2 conditions, $\mathscr{D}_G$ = 9.64 ft^2/sec.

After examining the available gas dispersion correlations, the LPMEOH data were fit to different variable groupings. The best fit resulted in a correlation of the following form (average error of 21.4% for cases 1 through 5):

$$\mathscr{D}_G = 4.64\, D^{1.5}\, U_G^{1.8} \qquad (37)$$

The data did not exhibit a strong dependency on gas holdup, so the data were fit only to outlet gas velocity. The various column diameter dependencies reported in the literature range from 1.3 to 2.0, with several authors using 1.5. Since our data were from one column, the column diameter dependency is arbitrary.

As previously noted, the Henry's Law coefficient may be inferred from the bulk velocity in the slurry. **Figure IV.C.2-3** is a plot of the Henry's Law coefficient for each injection versus the slurry height for that injection. Each cluster of points corresponds to

FIGURE IV.C.2-2

Gas Dispersion vs Outlet Superficial Velocity

Curve Fit Dg = a*(Ug)**B: All Cases

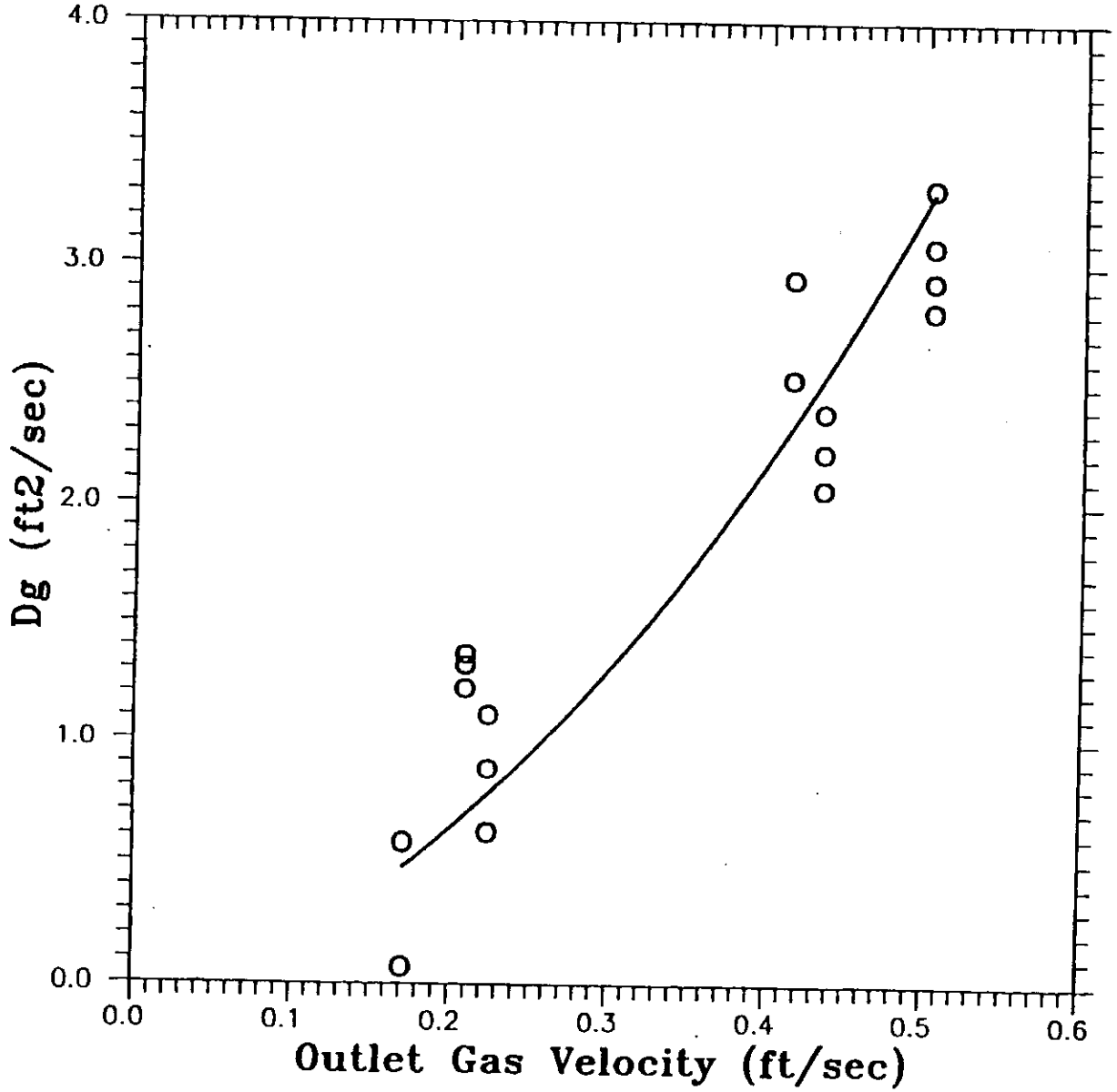

Figure: IV.C.2-3

Apparent Henry's Law Coefficient

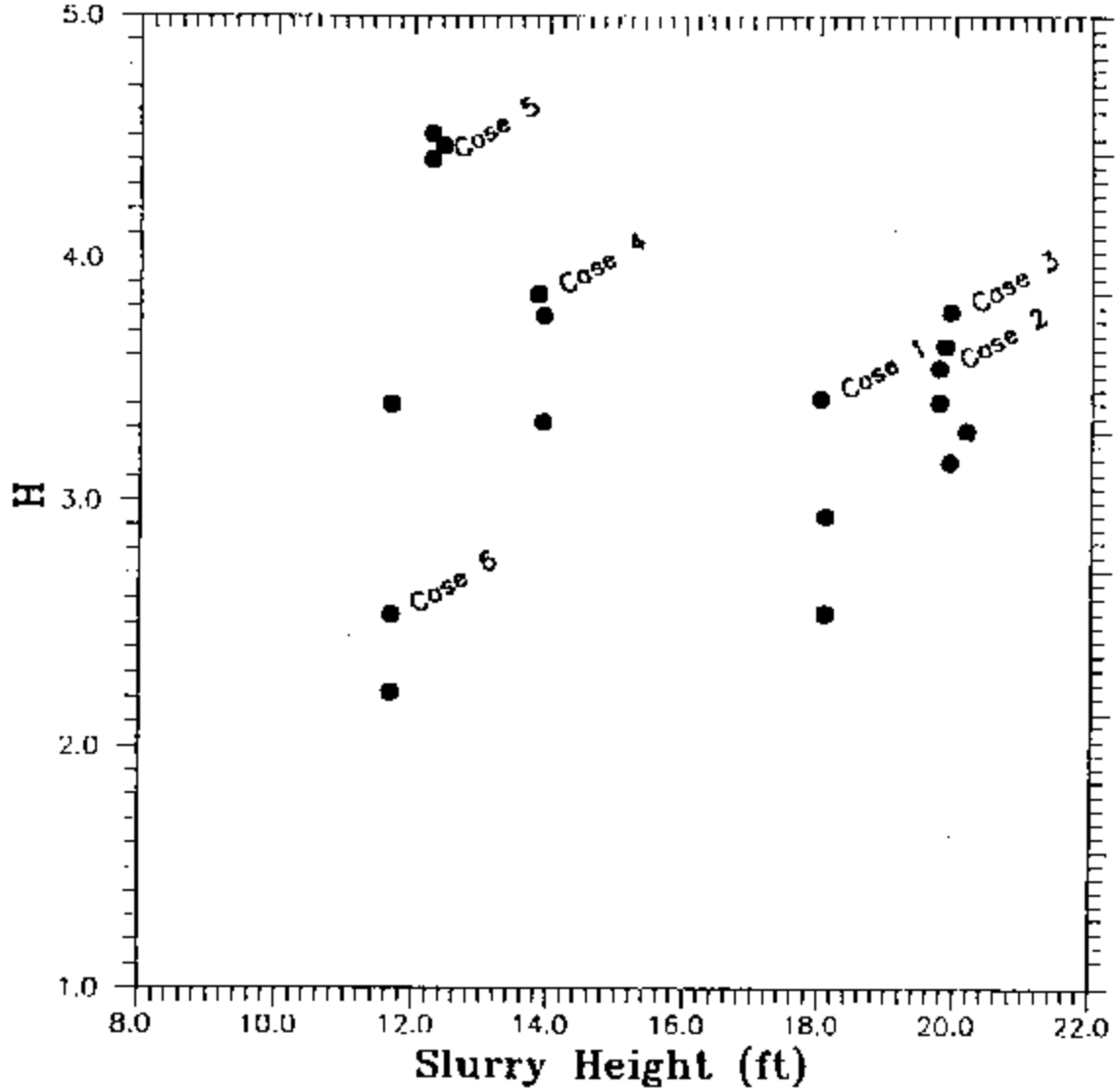

one injection of case 1 through 6 as labeled. The value of the experimental coefficient H varies between 2 and 4.5 with the bulk of the data predicting values between 3.2 and 4.0. The Peng-Robinson equation of state places the value for Argon at 5.4. This thermodynamic model has previously shown good reliability. The increasing scatter at low slurry levels (cases 4, 5, and 6) suggest that the bottom 10 feet of the reactor behave differently than the rest of the column. The lower measured values of H may imply that more argon is dissolving into the slurry than expected. Adsorption onto the catalyst might account for the enhanced phase transfer, though the effect has not been quantified.

3. Equivalent CSTR Models

The gas phase mixing was described earlier using the series-of-CSTR's model. The translation of a plug flow dispersion model to a series of CSTR's is given by Levenspiel [13] as

$$n^{-1} = 2\ Pe^{-1} - 2\ Pe^{-2}\ (1-\exp(-Pe)) \qquad (38)$$

where the Peclet number is defined as $(U_G\ L)/(\epsilon_G\ \mathcal{D}_G)$. Figure IV.C.3-1 is a plot of the number of tanks per unit length for gas phase mixing versus superficial gas velocity. The number of tanks, n, is calculated from the dispersion coefficients reported above for the gas phase. The more reliable measurements, based on the scatter of data, are those of cases 1, 2 and 3, the high slurry level runs.

The number of tanks varies between about 0.20 per foot and 0.35 per foot for cases 1, 2, 3 and 4. There is considerable scatter for the other 2 cases. While the tanks-in-series analysis done previously showed an increasing number of CSTR's with increasing gas velocity, this translation of gas dispersion to number of tanks shows no strong trend. The scatter in the data is too strong to suggest any effect of gas velocity.

To relate the number of tanks to the liquid dispersion coefficient, the relationship between the backflow cells model and the dispersion model must be utilized [14]. A comparison with the finite difference form of the dispersion equation suggests that, for uniform backflow cells, the axial dispersion coefficient is given by the equation

$$\mathcal{D}_L = (f_i\ L^2)/(n\ V_{TOTAL}) = f_i L_i^{\ 2}/V_i \qquad (39)$$

where V_i is the single cell volume, f_i is the flow rate between cells, and L_i is the axial length of a cell. The number of identical cells into which a given system is divided may be increased arbitrarily keeping the ratio f_i/n constant. The ability to break the column into zones of different mixing intensity without introducing great complexity is an advantage of

FIGURE IV.C.3) **Number of CSTRs per Length**
Based on Gas Dispersion vs Outlet Gas Velocity

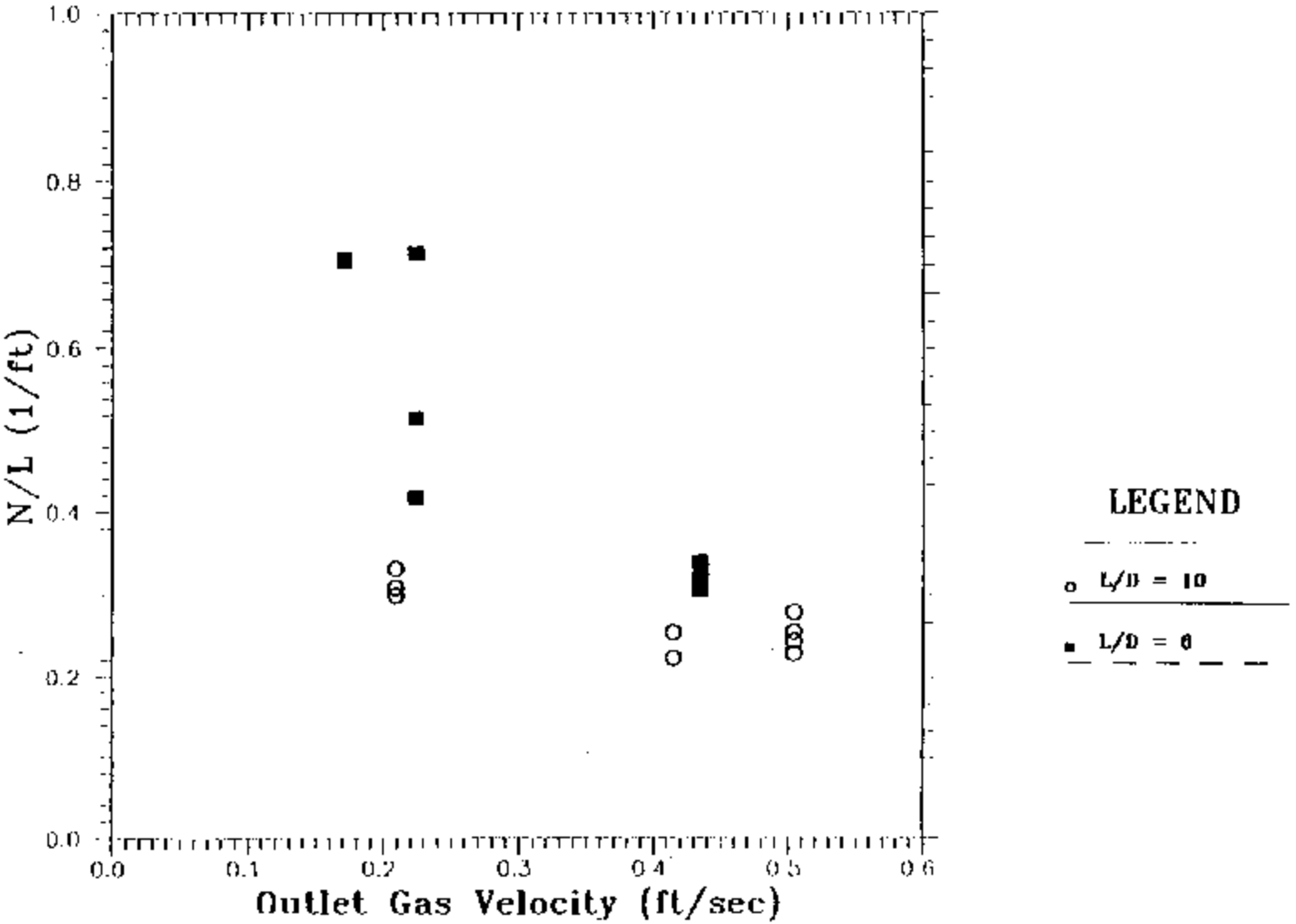

the backflow cell model. The measured value of the liquid dispersion coefficient, $\mathscr{D}_L$ = 3.7 ft^2/sec for case 7, translates to V_i/f_i = 13 sec for a three cell model. The average holdup time of the three cells in the model reported earlier was 13.8 sec, which is in good agreement. The backflow model could be used to iterate on the number of mixing cells given the dispersion characteristics of the liquid.

The number of CSTR's was next calculated from the effective dispersion coefficients used to determine $\mathscr{D}_G$. The statistical fit of $\mathscr{D}_{EFF}$ from all the detectors for each injection was used to calculate the effective Peclet number (based on U_{EFF} and $\mathscr{D}_{EFF}$) and the number of effective CSTR's. The calculated number of CSTRs are compared in **Table IV.C.3-1** and illustrated in **Figures IV.C.3-2 and IV.C.3-3** . By using $\mathscr{D}_{EFF}$ to calculate the number of CSTR's, the trends predicted by the tanks-in-series model were duplicated. That is, as superficial gas velocity increases, the number of CSTR's increases.

4. Scaleup Using the Axial Dispersion Model

The axial dispersion coefficients in both gas and liquid phases have been measured for the LaPorte methanol synthesis reactor, a slurry bubble column, and correlations were selected for scaleup.

The slurried catalyst solids and the solid tracer powder closely follow the liquid. Therefore, dispersion of the solids need not be considered separately. The liquid dispersion coefficient was determined to be 3.7 $\pm$ 0.2 ft^2/sec for a superficial gas velocity of 0.5 ft/sec, the single run condition studied. For scale-up, equation (32) is recommended with K = 0.667 to fit the measured value. In this way, the liquid dispersion coefficient is

$$\mathscr{D}_L = 0.667\ (g\ D^4 U_G)^{1/3} \qquad (40)$$

In the absence of a generally agreed upon or reliable correlation for gas dispersion in the literature, the LPMEOH data were fit to a dependency on outlet superficial gas velocity. The following correlation is recommended as the best available to characterize the dispersion of the gas phase in the LPMEOH slurry. The dependency on column diameter was chosen from literature recommendations, since the data analyzed was for one column diameter.

$$\mathscr{D}_G = 4.42\ \ D^{1.5}\ U_G^{\ 1.8} \qquad (41)$$

These correlations were tested for scaleup to a commercial scale reactor. Conditions for a typical commercial application are shown in Table IV.C.4-1 [16]. The reactor feed gas conditions are based on a 1000 psig Texaco gasifier firing Illinois No. 6 coal and are

taken from an EPRI sponsored report (No. AP2212). The dispersion coefficients for the gas and liquid phase were calculated using the previously recommended correlations (equations 40 & 41). From these values, an effective dispersion coefficient, as defined in equation 21, was estimated. This was translated to an effective number of tanks-in-series, using the Levenspiel relationship (equation 38). See Appendix H for the detailed calculations.

For the liquid phase $\mathscr{D}_L$ was estimated at 56.16 ft^2/sec and for the gas phase, $\mathscr{D}_G$ was calculated to be 106.52 ft^2/sec. The effective dispersion coefficient for the commerical scale reactor was 96.35 ft^2/sec and this translates to 1.22 CSTRs.

FIGURE IV.C.3-2

Number of CSTRs vs Outlet Superficial Velocity

Dispersion vs Tanks in Series Model: L/D= 9.5 - 10.8

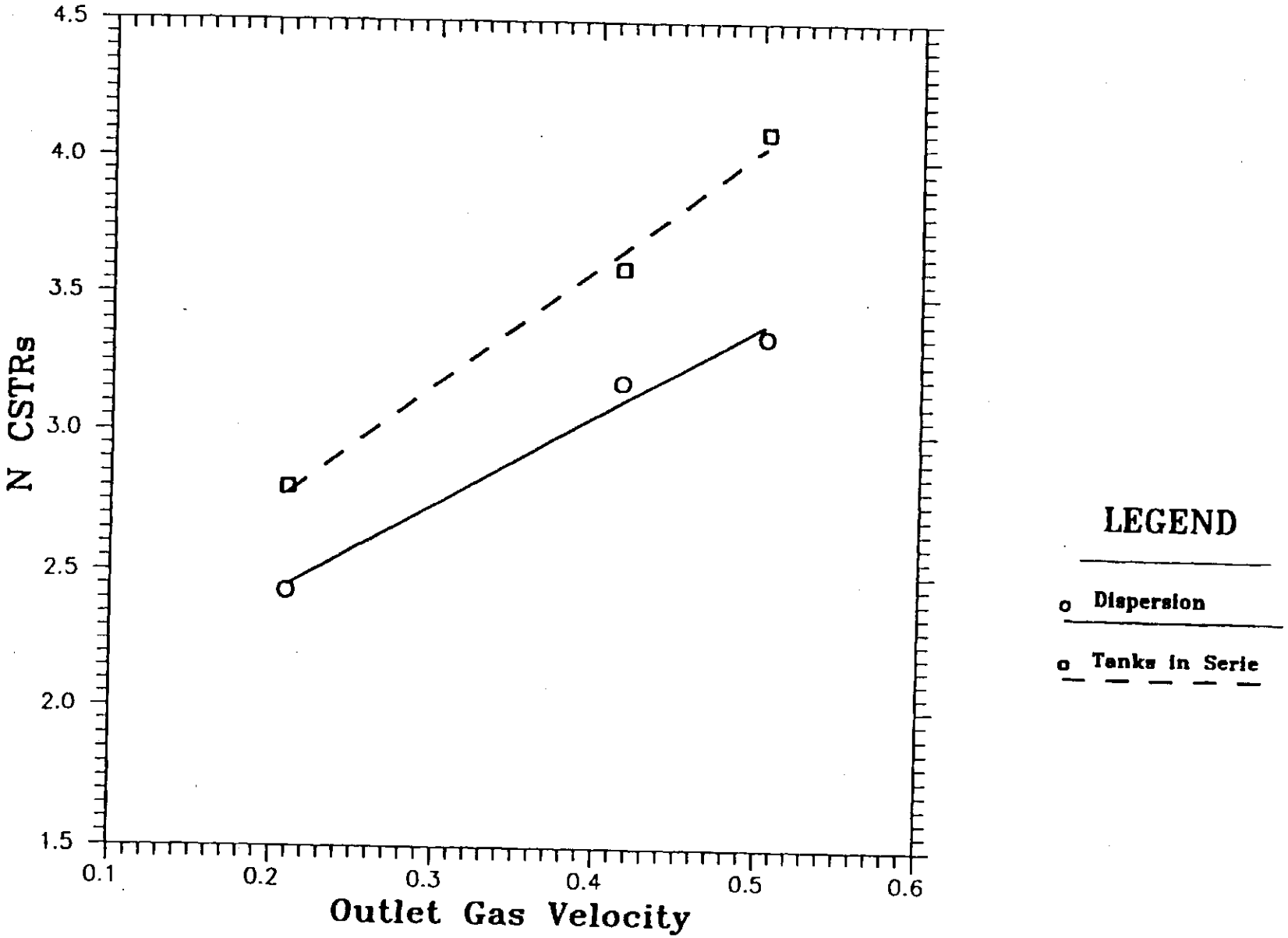

FIGURE IV.C.3-3

Number of CSTRs vs Outlet Superficial Velocity

Dispersion vs Tanks in Series Model: L/D= 6.18 - 7.56

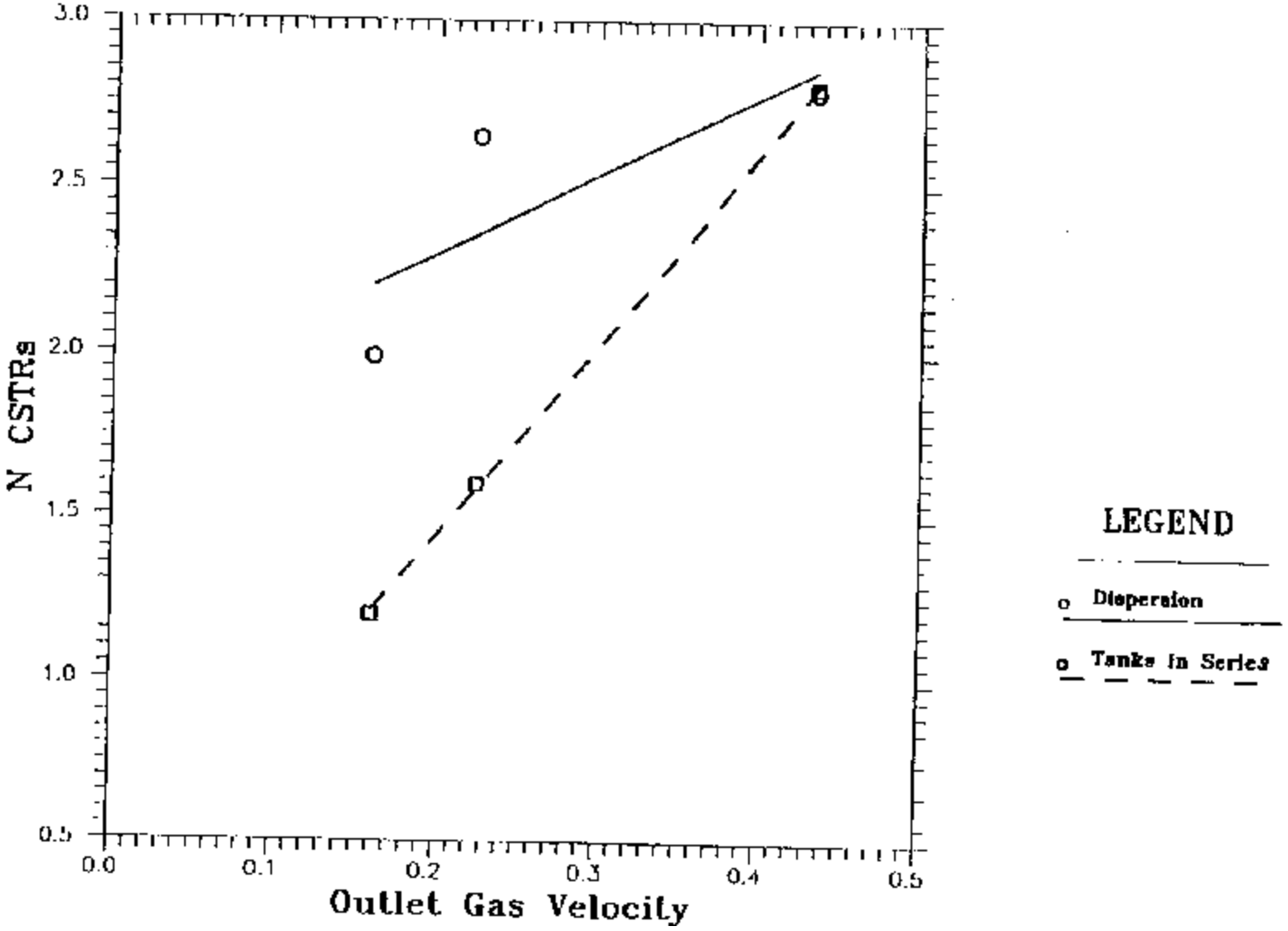

TABLE IV.C.3-1

COMPARISON OF THE NUMBER OF CSTR'S CALCULATED FROM AN "EFFECTIVE" DISPERSION COEFFICIENT WITH THE TANKS-IN-SERIES MODEL

Case No.	Inlet Gas Superficial Velocity ft/sec	Outlet Gas Superficial Velocity ft/sec	L/D	Axial Dispersion Model Ncstr	Tanks in Series Model Ncstr
6	0.19	0.171	6.22	1.99 ± 0.34	1.20 ± 0.1
1	0.25	0.209	9.64	2.43 ± 0.26	2.80 ± 0.4
5	0.25	0.224	6.53	2.65 ± 0.19	1.60 ± 0.5
2	0.50	0.415	10.53	3.18 ± 0.14	3.60 ± 0.5
4	0.50	0.435	7.42	2.79 ± 0.10	2.80 ± 0.3
3	0.60	0.504	10.62	3.35 ± 0.17	4.10 ± 0.9

TABLE IV.C.4-1

COMMERCIAL OPERATING AND PERFORMANCE PREDICTION

	Commercial Application
Reactor Feed Gas Conditions	
Flowrate, MSCFH	9024
Composition, mol%	
Hydrogen	36.6
Carbon Monoxide	53.5
Carbon Dioxide	8.8
Methane	0.1
Methanol	--
Nitrogen/Inerts	1.0
Reactor Design Conditions	
Temperature, °F	482
Pressure, psia	895
Internal Diameter, ft	12.8
Liquid Height, ft	42.8
L/D Ratio, ft/ft	3.4
Liquid Volume, cubic ft	5500
Gas Velocity, ft/sec	0.7
Space Velocity, Sl/hr kg	8000
Slurry Catalyst Conc., wt%	35
Reactor Performance	
Production Rate, TPD	560
Catalyst Productivity, gmol/hr kg	23.0
Conversion, %	
BTU (LHV)	17.1
Feed Gas Flow (SCFH)	12.9
Carbon Monoxide	11.9
Hydrogen	35.3